Supplementary Information 1

Decomposed SH-, SV-, and P-wavefields and their visualizations for interpretation of reproduced synthetic waves in the Osaka sedimentary basin, Japan, due to a Mw 5.6 earthquake beneath its edge

Hirotoshi Uebayashi[1] and Haruko Sekiguchi[2]

Supplementary information on the ordinary method identification errors in propagation direction and phase velocity

[1] Institute for Integrated Radiation and Nuclear Science, Kyoto University
[2] Disaster Prevention Research Institute, Kyoto University

Table of content:

Figure S1 Spatial distributions of propagation azimuth error for each semblance evaluation point indicated using different coloured circles, spatial distributions of the peak amplitude ratio of SH-waves to SV-waves in the decomposed wavefields indicated using different coloured circles, and scatter diagrams showing the relationship between the propagation azimuth error and the SH/SV amplitude ratio. All figures are for the frequency band 0.25–0.5 Hz (BP2) in three-time windows.

Figure S2 Same as the spatial error distributions and the scatter diagrams in Fig. S1, but for the relative error in the phase velocity taking the time window of 13.7 s in BP2

Ordinary method identification errors in propagation direction and phase velocity

By applying the semblance analysis to the full wavefield, the propagation characteristics such as the propagation azimuth and phase velocity for each wave type have been identified in many research cases. In subsection 4.1, we referred to these wave types as the SH-wave-like and the SV-wave-like. This method is referred to here as the ordinary method. On the other hand, the method used to identify the propagation characteristics of SH- and SV-waves from the decomposed wavefields using the semblance analysis is referred to as the exact method. In this part, errors in the propagation azimuths and phase velocities for the SH-wave-like and the SV-waves-like identified by the ordinary method are examined. Errors were evaluated as the differences between the values identified for decomposed SH- and SV-waves shown in subsections 4.2 and 4.3 (true values) and those identified by the ordinary method. Here, full wavefield means the waveform reproduced by the finite difference method. The parameters shown in Table 1 were also used in the semblance analysis for the full wavefield.

The two columns on the left-hand side in Fig. S1 show the propagation azimuth error which is the difference of the value determined by the ordinary method from the value obtained by the exact method in each of the SH- and SV-waves. The anticlockwise direction error is taken to be positive. The circle diameter is proportional to the peak amplitude of the stacked waveforms for each decomposed wavefield. However, the peak amplitude was normalised for each wave type and each time window.

The third column from the left in the figure shows distributions of the peak amplitude ratio of SH-waves to SV-waves in the decomposed wavefields. The circle diameter is proportional to the average of the peak amplitude of the SH- and SV-waves shown in the two columns on the left-hand side. The right-hand column in the figure shows the relationship between the propagation azimuth error and the SH/SV amplitude ratio. The pink circles indicate the error in the ORT component (corresponding to SH-waves), and the blue crosses indicate the error in the PAR component (corresponding to SV-waves). The size of the marks on the plot is proportional to the peak amplitude in the decomposed wavefield.

Focusing on the propagation characteristics in Area A for BP2, shown as a representative of the three frequency bands, which are strongly influenced by the shape of the sediment-bedrock interface, the errors in the ORT component corresponding to SH-waves were small and those in the PAR component corresponding to SV-waves were relatively large. This may be because the SH-wave amplitude was dominant over the SV-wave amplitude in this area. However, focusing on Area B, the errors in the PAR component were small and those in the ORT component were large, and the SV-wave amplitude was dominant over the SH-wave amplitude. Looking at the scatter diagram on the right-hand side of the figure, the variation in error distribution near an SH/SV amplitude ratio of 1 was larger for both components (circles and crosses). However, as the amplitude ratio became smaller or larger than 1, the variation became smaller, and there was a trend of convergence around 0. This trend was also confirmed in BP1 and BP3, although the figures are omitted. Overall, in the scatter diagrams, when the SH-wave or SV-wave amplitude was approximately three times larger than the other amplitude, the error was within 20–30° in many cases.

Looking at Fig. S2, which shows the relative error in the phase velocity instead of the propagation azimuth error in Fig. S1, the distributions of the colours representing the error and the scatter diagrams showing the relationship between the error and the SH/SV amplitude ratio show the same trends as the azimuth error distribution. In conclusion, the identification error for propagation azimuth and phase velocity based on semblance analysis for the full wavefield was found to become larger with increasing degree of interference between SH- and SV-waves (in other words, the closer to 1 the ratio of both waves in the full wavefield becomes). This problem is equivalent to the error evaluation when estimating Love-wave phase velocity from the horizontal components of microtremors in which both Love and Rayleigh waves are mixed. That is, unless the components due to Love waves (such as the rotational component in Eq. (3)) that are not affected by Rayleigh waves are extracted from the horizontal components of microtremors, the error in the identified Love-wave phase velocity will be large in a wavefield with Rayleigh waves that are comparable to Love waves in amplitude power. Therefore, the above conclusion can be interpreted as a limitation of the use of full wavefield data for estimating phase velocity and propagation azimuth.

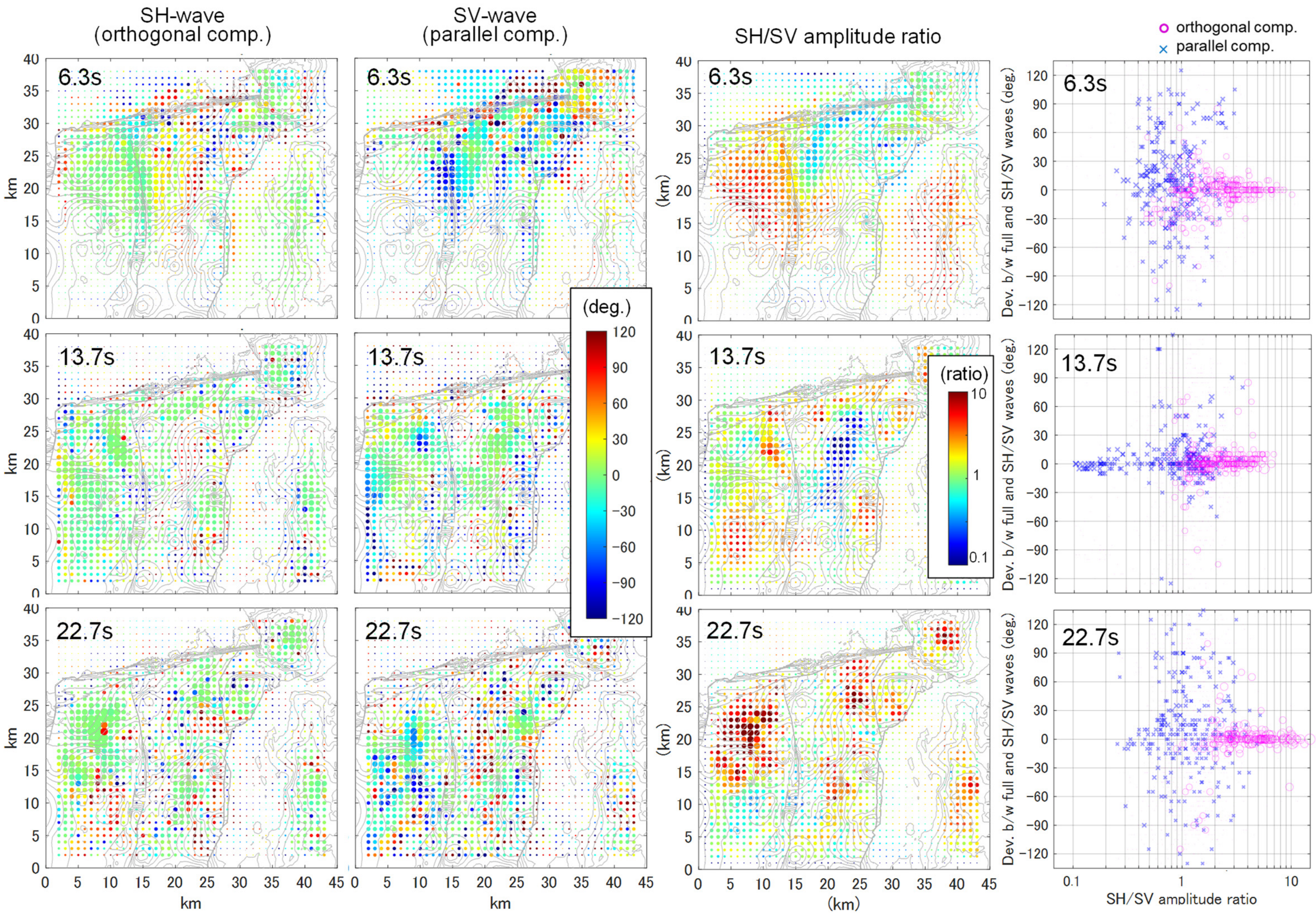

Figure S1 Spatial distributions of propagation azimuth error for each semblance evaluation point indicated using different coloured circles, spatial distributions of the peak amplitude ratio of SH-waves to SV-waves in the decomposed wavefields indicated using different coloured circles, and scatter diagrams showing the relationship between the propagation azimuth error and the SH/SV amplitude ratio. All figures are for the frequency band 0.25–0.5 Hz (BP2) in three-time windows.

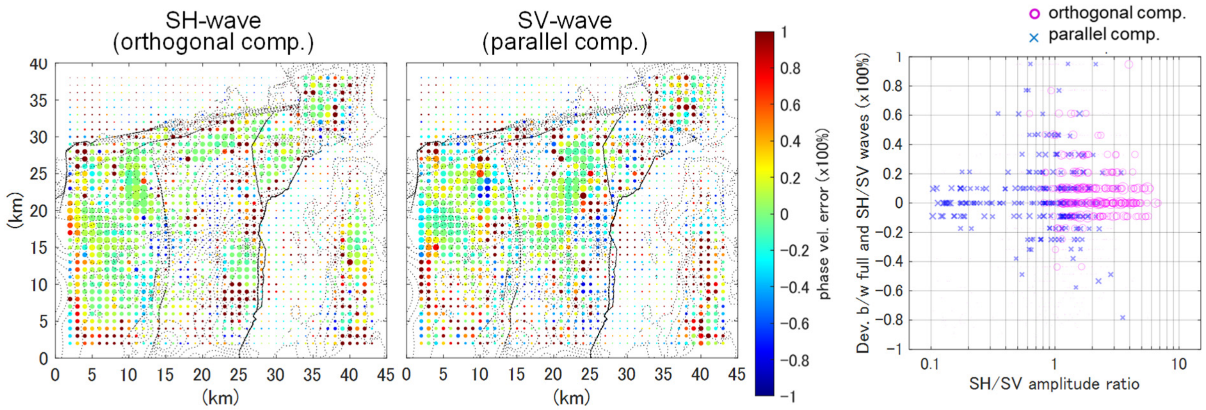

Figure S2 Same as the spatial error distributions and the scatter diagrams in Fig. S1, but for the relative error in the phase velocity taking the time window of 13.7 s in BP2.